Journal of Catalysis 264 (2009) 145–153

Contents lists available at ScienceDirect

Journal of Catalysis

journal homepage: www.elsevier.com/locate/jcat

Effect of pretreatment atmosphere on CO oxidation over α-Mn_2O_3 supported gold catalysts

Lu-Cun Wang, Lin He, Yong-Mei Liu, Yong Cao *, He-Yong He, Kang-Nian Fan, Ji-Hua Zhuang *

Shanghai Key Laboratory of Molecular Catalysis and Innovative Materials, Department of Chemistry, Fudan University, Shanghai 200433, PR China

ARTICLE INFO

Article history:
Received 3 March 2009
Revised 2 April 2009
Accepted 3 April 2009
Available online 6 May 2009

Keywords:
Supported gold catalyst
α-Mn_2O_3
CO oxidation
Pretreatment atmosphere
Deactivation

ABSTRACT

The microstructural properties of Au/α-Mn_2O_3 catalysts moderately pretreated under different atmospheres, i.e., O_2, He and H_2, in relation to their activities and stabilities on CO oxidation were investigated. The highest initial activity was obtained for the He-pretreated catalyst, which, however, suffered the most severe deactivation with time on stream. Pretreatment with O_2 resulted in the best stability and had the highest steady-state activity among the three catalysts. TEM results revealed that the pretreatment has a negligible effect on the gold particle size. While the formation of moderate surface oxygen vacancies before reaction was suggested to be responsible for the highest initial activity of He–Au/α-Mn_2O_3, overreduction of the oxide support could explain the inferior activity of the H_2-pretreated catalyst. Based on the XPS and in situ DRIFTS studies, the superior performance of the O_2-pretreated O_2–Au/α-Mn_2O_3 catalyst can be attributed to the creation of a specific oxygen-enriched interface leading to an enhanced metal–support synergy.

1. Introduction

Recently, oxide-supported gold catalysts have attracted tremendous research interest owing to their unique catalytic properties for various redox reactions, in particular, for CO oxidation under ambient conditions [1,2]. It is generally accepted that gold dispersed on reducible oxides is more active and stable than that supported on non-reducible oxides (SiO_2, Al_2O_3) [3]. Exceptionally high activities for CO oxidation have been reported for finely dispersed Au on reducible oxides, such as TiO_2 [4], CeO_2 [5], Fe_2O_3 [3,4], Co_3O_4 [4] and Mn_2O_3 [6,7]. The gold particle size along with the metal–support interaction/synergy has been suggested to play a decisive role in controlling the activity of the gold catalysts [1,2,8]. These two factors are largely determined by the preparation method and the activation or pretreatment conditions before reaction [4–8].

Among the various techniques used to prepare supported gold catalysts, deposition–precipitation (DP) with the most common gold precursor, $HAuCl_4$, appeared to be the most suitable method to achieve highly active catalysts [1–4]. With this method, it is possible to obtain very small gold metal particles (2–3 nm) that are highly active for CO oxidation. The main feature in the DP technique is the deposition of the gold precursor on the support, in which one of the major factors is the appropriate pH value [9]. Subsequent thermal treatment following the drying step is generally required for the genesis of active Au species [10,11]. Although there is no general agreement on the optimal calcination temperature for the supported Au particles for CO oxidation, it is frequently observed that calcination at temperatures above 673 K results in a deteriorated activity, which has been attributed to sintering and/or a change in the shape of the particle [10–13].

As for the additional pretreatment to activate the gold catalysts, it has been reported that pretreatment gas conditions can exert a significant influence on the final structure and activity of the supported gold catalysts [14–18]. For example, Gardner et al. [14,15] reported that the pretreatment of Au–MnO_x in He at 328 K resulted in a significant enhancement in the activity for CO oxidation, which may be due to enrichment in the Au and O contents on the surface of this catalyst as revealed by XPS. Zanella and Louis [10] and Tsubota et al. [16] showed that a moderate thermal treatment of Au/TiO_2 catalyst under hydrogen or argon leads to smaller gold particles than that under air. On the other hand, Park and Lee [17] found that the rate of CO oxidation over Au/TiO_2 pretreated in H_2 is lower than that inertly pretreated, and the preoxidized one yields the highest activity. More recently, Ho and Yeung [18] have reported that O_3-pretreated Au/TiO_2 catalyst exhibited a better Au dispersion and enhanced stability compared with O_2-pretreated Au/TiO_2.

Notwithstanding the extensive research on Au catalysts, the structural effects associated with the activation process have not been well understood, in particular, the oxidation state of gold and the effect on the metal–support interface. In the present paper, we focus on the effect of pretreatment atmosphere on the

* Corresponding authors. Fax: +86 21 65643774.
E-mail addresses: yongcao@fudan.edu.cn (Y. Cao), jihuaz@fudan.edu.cn (J.-H. Zhuang).

0021-9517/$ - see front matter © 2009 Elsevier Inc. All rights reserved.
doi:10.1016/j.jcat.2009.04.006

activation, deactivation and regeneration of a model Au/α-Mn_2O_3 catalyst, which is one of the best catalysts for CO oxidation, even in the presence of water or hydrogen [6,7]. We use XPS, TEM, XRD and in situ DRIFTS coupled with CO adsorption to study the effect of various pre-treatments, i.e., reductive, oxidative and inert atmosphere, on the structure and morphology of the gold particles, manganese oxide support and the metal–support interaction.

2. Experimental

2.1. Catalyst preparation

α-Mn_2O_3 was prepared by the direct thermal decomposition of $MnCO_3$ powder (Aldrich) in static air [19]. Gold was deposited on the as-synthesized α-Mn_2O_3 by DP using urea as the precipitating agent [20]. Typically, 0.55 g of α-Mn_2O_3 was added to an aqueous solution with the desired amount of $HAuCl_4$ and urea (urea/Au = 100, molar ratio). The suspension was then heated to 363 K and stirred for 4 h, followed by filtering and washing several times with deionized water to remove Cl^-. The resulting solid product was dried overnight before calcination at 573 K for 4 h in static air. The gold loading of the as- prepared catalyst was 2.9 wt% as determined by ICP-AES.

2.2. Catalyst activity tests and kinetic measurements

The catalysts were evaluated at atmospheric pressure using a fixed bed quartz reactor (i.d. 3 mm). The weight of the catalyst was 20 mg, and the total flow rate of the reaction gas was 50 mL min^{-1}, with a composition of 1%CO–20%O_2 (balanced with He). Prior to the reaction, the catalysts were pretreated with 30 mL min^{-1} of He, O_2 or H_2 at 473 K for 0.5 h. For the sake of clarity, the three as-treated catalysts were referred to He–Au/α-Mn_2O_3, O_2-Au/α-Mn_2O_3 and H_2-Au/α-Mn_2O_3. Kinetic measurements were performed under differential reaction conditions, with typically 2 mg catalyst powder. To limit the conversion to values typically between 5% and 20%, the catalysts were diluted with chemically inert α-Al_2O_3. The reactions were carried out with 100 mL min^{-1} of 1%CO–20%O_2 balanced with He. Kinetic data were acquired after 120-min reaction. The composition of the influent and effluent gas was detected with an online GC-17A gas chromatograph equipped with a TDX-01 column. The conversion of CO was calculated from the change in CO concentrations in the inlet and outlet gases.

2.3. Catalyst characterization

The BET specific surface areas of the calcined catalysts were determined by adsorption–desorption of nitrogen at liquid nitrogen temperature, using Micromeritics TriStar 3000 equipment. The X-ray powder diffraction (XRD) was carried out on a Bruker AXS D8 Avance X-ray diffractometer with nickel-filtered Cu $K\alpha_1$ radiation (λ = 1.540562 Å) with a voltage and current of 40 kV and 20 mA, respectively. Chemical analysis was performed by inductively coupled plasma (ICP) atomic emission spectroscopy using a Thermo Electron IRIS Intrepid II XSP spectrometer. A JEOL 2011 microscope operating at 200 kV equipped with an EDX unit (Si(Li) detector) was used for the TEM investigations.

XPS data were obtained with a Perkin Elmer PHI 5000C system equipped with a hemispherical electron energy analyzer. The adventitious carbonaceous C 1s line (284.6 eV) was used as the reference to calibrate the binding energies (BEs). Prior to the XPS characterization, the Au/α-Mn_2O_3 catalyst was pretreated under different atmospheres as in the case of activity measurements. The diffuse reflectance infrared Fourier transform spectroscopy (DRIFTS) experiments were carried out on a Bruker Vector 22 FT-IR spectrometer equipped with a MCT detector and Harrick diffuse reflectance accessory. In situ pretreatment was performed with 30 mL min^{-1} of He, O_2 or H_2 at 473 K for 0.5 h, as in the case of activity measurements. Background signals from gas-phase CO were subtracted before the spectra were reported.

3. Results and discussion

3.1. Structural characterization

Fig. 1 shows the XRD patterns of various Au/α-Mn_2O_3 catalysts. For the samples pretreated in O_2 or He, only the well-defined diffraction peaks of α-Mn_2O_3 (bixbyite, JCPDS 41-1442) can be identified. In contrast, additional peaks at $2\theta = 36.2°$ and 44.4° characteristic of Mn_3O_4 phase emerged in the XRD pattern of the H_2-pretreated sample (Fig. 1c), indicating that a partial reduction of the parent support has occurred. In addition, no distinct Au reflections are visible in the XRD patterns of any samples, owing to the fact that the strongest reflection from gold overlaps with that of α-Mn_2O_3 at $2\theta = 38.2°$ [6]. TEM was then used as a complementary technique to examine the structures of Au particles. Representative TEM images for various samples are shown in Fig. 2. It can be observed that for all samples, gold particles with a narrow size distribution in the range of 1 ~ 3 nm are finely dispersed on the surface of the support. The average gold particle size is estimated to be ca. 2.0, 2.0 and 1.9 nm for the samples pretreated in O_2, He and H_2, respectively (see Table 1), which clearly indicates that the nature of gas has a negligible effect on the gold particle size.

3.2. Chemical state and surface composition

XPS characterization was performed to investigate the chemical state of various Au/α-Mn_2O_3 catalysts. The Au 4f, Mn 2p and O 1s XP spectra of all three samples are presented in Fig. 3a–c, respectively. The detailed XPS parameters are summarized in Table 2. As illustrated in Fig. 3a, quantitative deconvolution of the Au 4f peaks revealed ca. 25% contribution from partially oxidized Au species (85.6 eV) [21] for the O_2-pretreated sample and the amount of positively charged gold species in the three samples decreased in the following order: O_2-Au/α-Mn_2O_3 > He–Au/α- Mn_2O_3 > H_2-Au/α-Mn_2O_3 (see Table 2). This indicates that conditioning in reductive atmosphere can lead to the formation of higher fraction of metallic

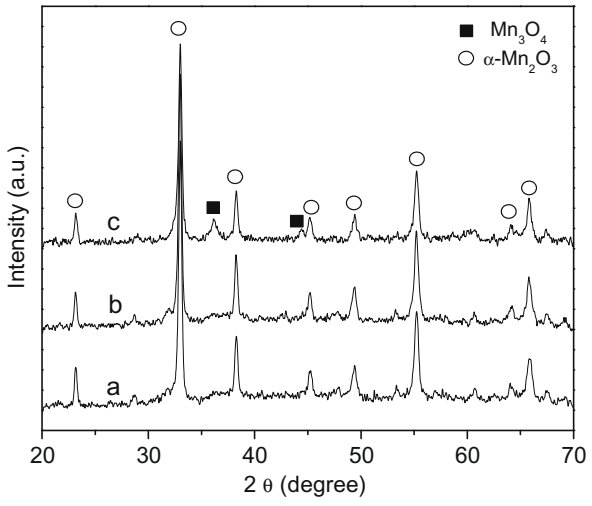

Fig. 1. XRD patterns of various Au/α-Mn_2O_3 catalysts: (a) O_2–Au/α-Mn_2O_3, (b) He–Au/α-Mn_2O_3 and (c) H_2–Au/α-Mn_2O_3.

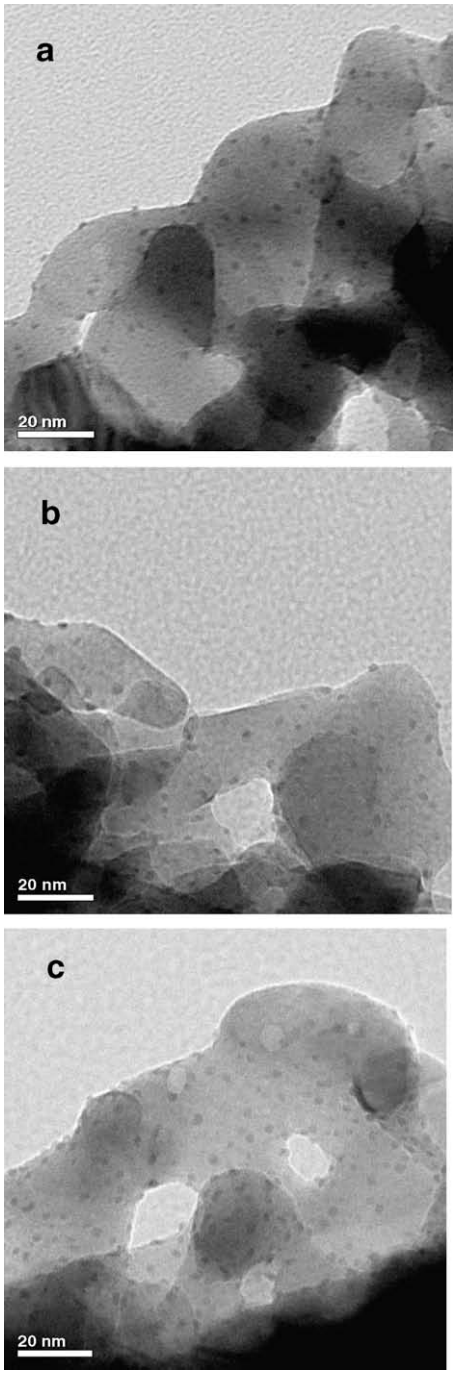

Fig. 2. TEM images of various Au/α-Mn_2O_3 catalysts: (a) O_2–Au/α-Mn_2O_3, (b) He–Au/α-Mn_2O_3 and (c) H_2–Au/α-Mn_2O_3.

Table 1
Physicochemical properties, catalytic activities and activation energies for various Au/α-Mn_2O_3 catalysts pretreated under different atmospheres.

Catalyst	d_{Au}[a] (nm)	T_{50}[b] (K)	r_{Au}[c] ($mmol_{CO}\ g_{Au}^{-1}\ s^{-1}$)	E_a (kJ mol^{-1})
O_2–Au/α-Mn_2O_3	2.0 ± 0.3	261	2.97	24
He–Au/α-Mn_2O_3	2.0 ± 0.4	252	2.31	19
H_2–Au/α-Mn_2O_3	1.9 ± 0.4	283	1.36	21

[a] Average gold particle size estimated by statistical analysis from TEM results.
[b] The temperature at which the conversion was 50%.
[c] The mass specific reaction rate of CO oxidation at 323 K.

Au^0. It may be noted that the high vacuum required for XPS and the energy of the soft X-rays could lead to the reduction of a fraction of cationic gold species [22]. Therefore, the real percentages of positive gold atoms that are present before analysis may be underestimated by XPS. Furthermore, it is worthwhile to note that it is difficult to determine the chemical state of Mn in the support, because the Mn 2p XPS spectra for the three samples in Fig. 3b show very similar Mn $2p_{3/2}$ peaks with the same binding energy (BE) at 641.3 eV. In addition, the extent of Mn 3s multiple splitting commonly used in the determination of Mn valences [23] cannot be obtained for the present system due to the superposition of Au 4f and Mn 3s peaks.

The surface compositions in Table 2 show that the pretreatment of Au/α-Mn_2O_3 under H_2 resulted in much smaller Au/Mn molar ratio than the treatment under O_2 or He, while similar Au/Mn ratios were obtained with the latter two gases. Considering the slightly smaller gold particle size of H_2-Au/α-Mn_2O_3 (see Fig. 2 and Table 1), one possible explanation could be the partial encapsulation of Au nanoparticles by manganese oxides as a result of strong metal–support interaction (SMSI). This scenario is reinforced by the fact that the in situ DRIFT CO adsorption studies (see below) show an obviously reduced intensity for H_2-Au/α-Mn_2O_3 as compared with other samples. Recently, by using XPS coupled with UV photoelectron spectroscopy (UPS), Guczi et al. [24] have observed a gradual decrease in the photoemission intensity for Au as opposed to Fe species upon vacuum annealing of a Au/FeO_x/SiO_2/Si(100) model system at temperatures above 773 K. Such a phenomenon has been rationalized by migration of the partially reduced iron oxide species leading to a partial encapsulation of Au particles.

Further information can be obtained from the O 1s spectra as shown in Fig. 3c. For each sample, the O 1s spectrum contains a main peak at ca. 529.4 eV characteristic of the lattice oxygen [14] along with a distinct shoulder at ca. 531.5 eV assignable to a mixture of hydroxyl groups and adsorbed water on the surface of the catalysts [14,25]. The peak deconvolution results as shown in Table 2 indicate a higher fraction of surface hydroxyl groups or chemisorbed water on the reductively pretreated sample compared with those pretreated in oxidative or inert atmosphere. On the other hand, the molar ratios of surface lattice oxygen (O_L, 529. 4 eV) to Mn for all samples are smaller than the stoichiometric value in Mn_2O_3 (1.5), inferring the presence of oxygen vacancies on the surface of the catalysts which, however, are filled by water or hydroxyl groups. The smallest O_L/Mn ratio was detected for H_2–Au/α-Mn_2O_3 (0.88), indicating a substantial reduction in the oxide support, in good agreement with the XRD results.

3.3. CO oxidation activity, reaction kinetics and stability

Fig. 4a displays the temperature dependence of the CO conversions for various catalysts. For comparison, the activity of the as-synthesized Au/α-Mn_2O_3 without pretreatment is also included. It is clear that the activity of Au/α-Mn_2O_3 is highly sensitive to the pretreatment atmosphere. Pretreatment in He or O_2 led to notably improved activity as compared with the unpretreated catalyst, whereas reductive pretreatment deteriorated the activity. Of all Au/α-Mn_2O_3 catalysts investigated, He–Au/α-Mn_2O_3 shows the highest activity for CO oxidation. The temperature at which the conversion was 50% (T_{50}) for He–Au/α-Mn_2O_3 is 252 K (Table 1), ca. 30 K below that for H_2–Au/α-Mn_2O_3. On the other hand, kinetic studies showed that all catalysts have similar activation energies (E_a), as reflected by the Arrhenius plots presented in Fig. 4b. This result suggests that different pretreatment conditions do not change the reaction mechanism of CO oxidation over the Au/α-Mn_2O_3 catalysts. It is also interesting to note that in contrast to the activity trend (light-off test) obtained from Fig. 4a, the

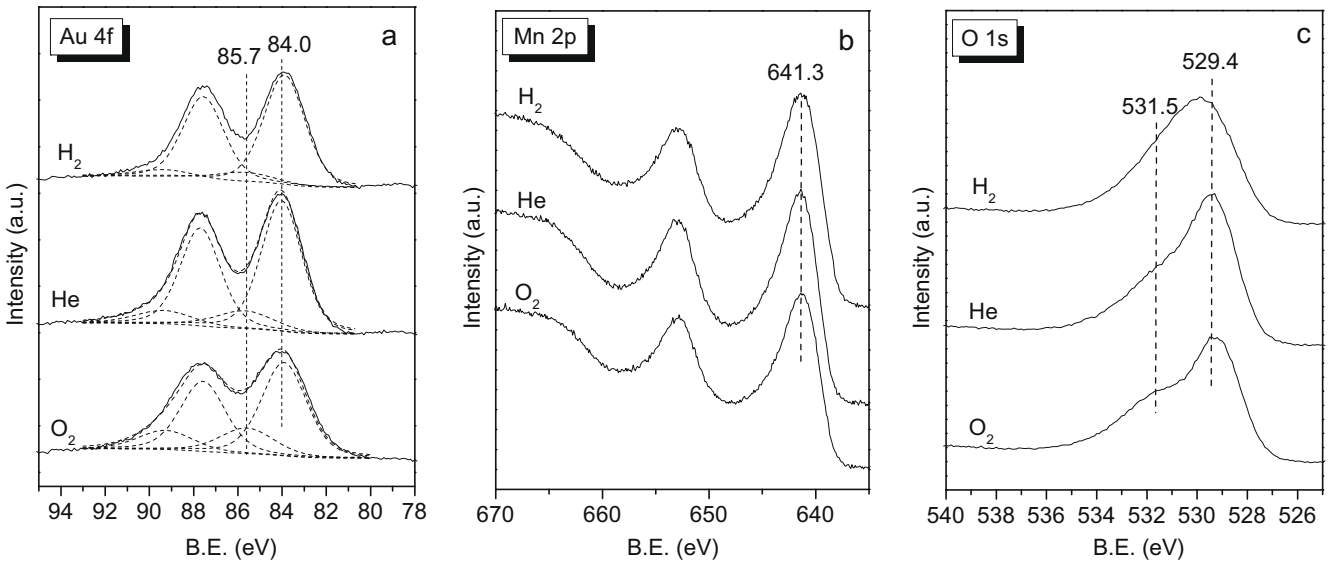

Fig. 3. XPS spectra of various Au/α-Mn_2O_3 catalysts. (a) Au 4f, (b) Mn 2p and (c) O 1s.

Table 2
XPS results of various Au/α-Mn_2O_3 catalysts pretreated under different atmospheres.

Catalyst	BE of Au $4f_{7/2}$ (eV)	$Au^{\delta+}$ (%)	BE of Mn $2p_{3/2}$ (eV)	(OH + H_2O)%[a]	Au/Mn	O_L/Mn[b]
O_2–Au/α-Mn_2O_3	83.9	25	641.4	35	0.093	1.45
He–Au/α-Mn_2O_3	84.0	16	641.4	36	0.091	1.30
H_2–Au/α-Mn_2O_3	83.9	10	641.3	54	0.082	0.88

[a] Proportion of OH groups and chemisorbed H_2O estimated from the O 1s spectra.
[b] O_L, surface lattice oxygen.

oxidative pretreatment gave the highest activity in terms of the reaction rates at steady state (after 2-h reaction).

Fig. 5 illustrates the deactivation of the various pretreated Au/α-Mn_2O_3 at 303 K for 2 h of CO oxidation reaction. The activities in Fig. 5a are described by the mass specific rate under differential reaction conditions. Fig. 5b shows the deactivation on a relative scale, relative to an initial activity of 100%. It is interesting to note that O_2–Au/α-Mn_2O_3 showed the best stability among the studied catalysts, with activity decayed by 38% after 120 min on stream. In contrast, the most severe deactivation occurred on He–Au/α-Mn_2O_3, with a loss of activity by 89% during the same period. The deactivated catalyst was then regenerated by He stream (with the same condition as that for the fresh sample) with largely restored initial activity. Interestingly, the stability of the regenerated He–Au/α-Mn_2O_3 was notably improved, with activity decayed by 76% after 120-min reaction. As for the catalyst pretreated with H_2, a severe deactivation was observed in the initial 20 min. However, the deactivation rate slowed down significantly afterwards, and the activity loss for H_2–Au/α-Mn_2O_3 was 78% in 120 min. It turns out that the steady-state activity follows the decreasing order of O_2–Au/α-Mn_2O_3 > He–Au/α-Mn_2O_3 > H_2–Au/α-Mn_2O_3.

3.4. In situ DRIFTS measurements

To better understand the origin of the different catalytic behaviours with various pretreatments, we studied the surface feature of the samples by DRIFTS, a powerful technique that can provide many valuable insights into the mechanism of heterogeneous catalytic reactions, especially under in situ conditions [26–29]. In this work, DRIFT spectra were collected to gain direct information about the initial state of the Au/α-Mn_2O_3 catalysts after various conditionings. In addition, CO adsorption on differently pretreated Au/α-Mn_2O_3 catalysts and the further evolution of reaction intermediates along with side products during CO oxidation were also investigated.

3.4.1. Initial states of various catalysts

To examine the initial surface feature of various Au/α-Mn_2O_3 catalysts, DRIFT spectra were collected as shown in Fig. 6. It can be seen that with reductive pretreatment, the broad band at 3300 ~ 3500 cm^{-1}, characteristic of molecularly adsorbed water or surface OH groups, is significantly stronger than those pretreated with oxidative and inert atmospheres. This is in good agreement with the XPS results. Moreover, the H_2-pretreated sample also shows much stronger bands in the carbonate region (1200 ~ 1700 cm^{-1}) as compared with the He- or O_2-pretreated samples, indicating promoted surface carbonate decomposition in the presence of O_2 or He. These findings are in line with the results reported by Denkwitz et al. for CO oxidation over Au/TiO_2 catalyst [30], where the growth of carbonate species was found markedly suppressed in an O_2-rich atmosphere. It is worth mentioning here that hydrogen has also been suggested to have beneficial effects in the removal of surface carbonates during CO oxidation for various gold catalysts [30,31]. However, it should be pointed out that this effect only works indirectly by producing water through hydrogen oxidation, based on the fact that water can facilitate the conversion of poisoning carbonates into thermally less stable bicarbonates [30–32].

3.4.2. CO adsorption studies

Fig. 7 shows the DRIFT spectra for CO adsorption on various catalysts after in situ pretreatment under different atmospheres. The adsorption of CO on O_2–Au/α-Mn_2O_3 for 5 min resulted in a strong band at ca. 2108 cm^{-1} with a small shoulder at higher frequency of ca. 2123 cm^{-1}. The former band is generally attributed to CO adsorption on the step/kink defect sites of the oxide-supported gold nanoparticles (Au^0–CO) [33,34], while the latter is associated with CO adsorption on positively polarized gold species ($Au^{\delta+}$–CO), which most likely result from the spillover of oxygen or OH groups from the support onto the Au nanoparticles [27,35]. Such CO

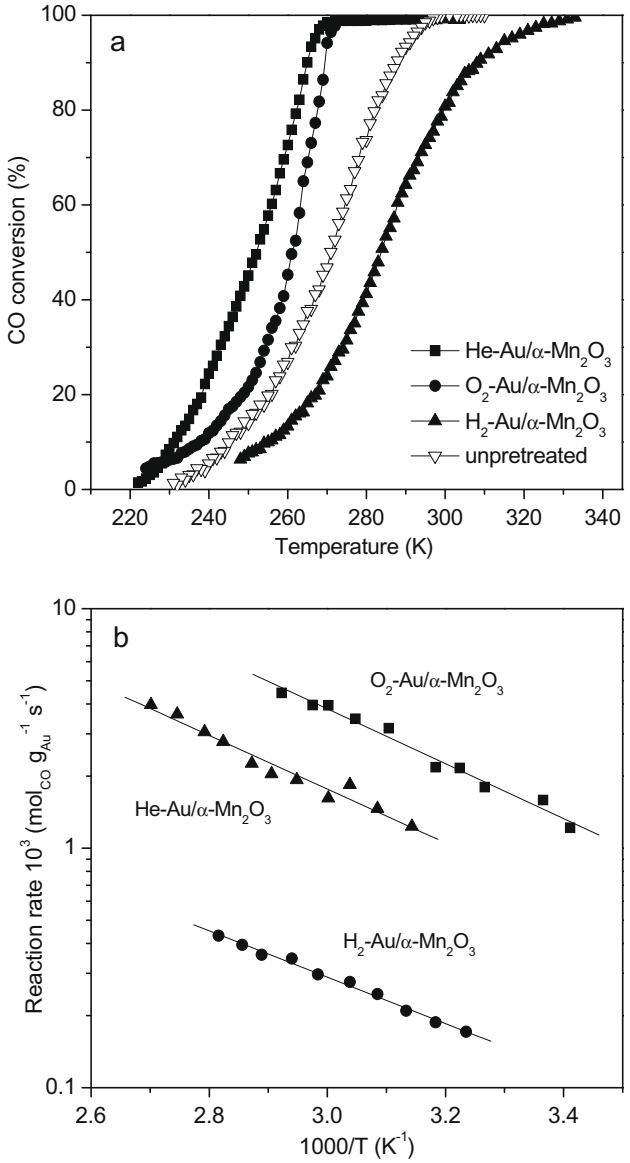

Fig. 4. (a) CO oxidation activity of Au/α-Mn_2O_3 catalysts pretreated with different conditions. Reaction conditions: 20 mg catalyst, 1%CO–20%O_2 balanced with He (50 mL min^{-1}). (b) Arrhenius plots of the reaction rate vs. 1/*T* for CO oxidation over various Au/α-Mn_2O_3 catalysts.

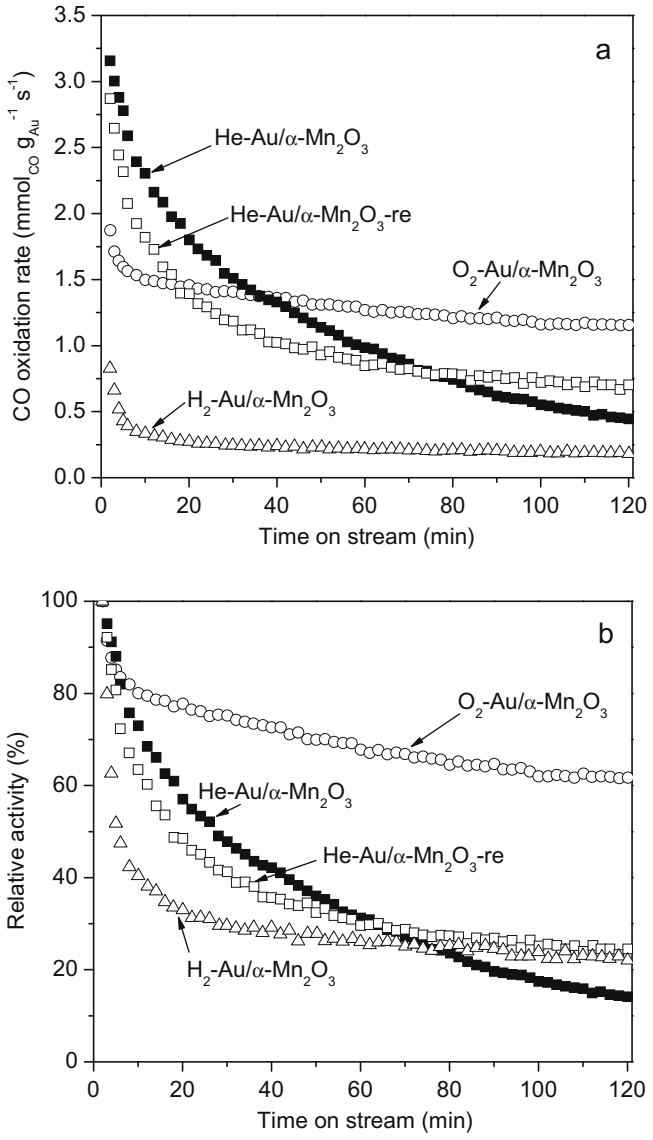

Fig. 5. Evolution of the mass specific CO oxidation rate (a) and the relative activity (b) on differently pretreated Au/α-Mn_2O_3 catalysts for 120 min on stream. Reaction conditions: 2 mg catalyst, 303 K, 1%CO–20%O_2 balanced with He (100 mL min^{-1}). He–Au/α-Mn_2O_3-re refers to He–Au/α-Mn_2O_3 after regeneration.

adsorption bands have also been observed on the Au/TiO_2 [36] and Au/CeO_2 [5] catalysts under similar conditions.

As compared with the O_2-pretreated sample, the Au^0–CO band is considerably weaker on He–Au/α-Mn_2O_3. This observation indicates less presence of defective gold sites on the He-pretreated sample. CO adsorption was also performed on the regenerated He–Au/α-Mn_2O_3. It is interesting to find that the intensity of the $Au^{\delta+}$–CO band increased notably, with that of the Au^0–CO band almost unaltered as compared with that of the fresh He–Au/α-Mn_2O_3. An increase in the positively charged gold sites can be understood by the fact that excess oxygen is present under reaction conditions. The H_2–Au/α-Mn_2O_3 sample shows the weakest CO adsorption band at 2101 cm^{-1} along with a shoulder at lower frequency of 2087 cm^{-1}. This shoulder peak could be ascribed to CO adsorption on negatively charged gold species ($Au^{\delta-}$–CO). Bands in a similar region have also been reported by Boccuzzi et al. [26] in a study of CO adsorption on a prereduced Au/TiO_2 sample, in addition to the "normal" peak at 2100 cm^{-1}. This distinct feature was proposed to arise from the reduction of the support by H_2 with transferring negative charge to the gold particles [26], which leads to an increased back-donation and hence to a weakening of the C–O bond.

3.4.3. State of the catalysts during CO oxidation reaction

The accumulation of adsorbed surface species on various catalysts during CO oxidation reaction was also followed by in situ DRIFT measurements. Fig. 8a illustrates the evolution of the full spectra recorded on O_2–Au/α-Mn_2O_3 during the reaction, with the enlarged details of the carbonate and CO_2/CO regions being presented in Fig. 8b–d. The spectra reveal the characteristic peaks of Au^0–CO at 2115 cm^{-1}, the bands of gaseous CO_2 at 2340 and 2360 cm^{-1} and a set of broad bands in the range of 1200–1750 cm^{-1}. The bands at 1517, 1338, 1480 and 1380 cm^{-1} are commonly assigned to the C=O, asymmetric O–C–O stretch vibration of bidentate carbonates, the symmetric and asymmetric O–C–O stretch vibration of monodentate carbonates [37], respectively. It is important to remark that the general features were

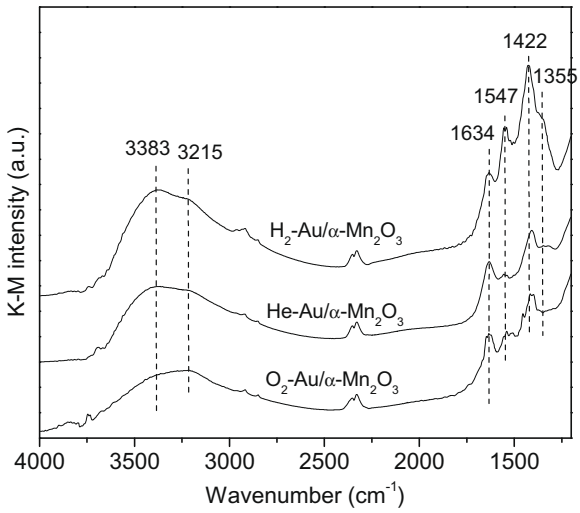

Fig. 6. DRIFT spectra of Au/α-Mn_2O_3 catalysts after various pretreatments.

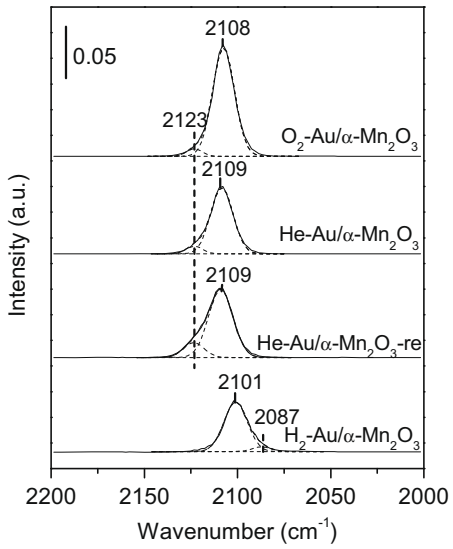

Fig. 7. DRIFT spectra of CO adsorption on various Au/α-Mn_2O_3 catalysts after CO adsorption for 5 min.

similar for all samples, while the characteristic frequencies and the intensities as well as their evolution during reaction were appreciably different. For instance, the CO related peaks appear at 2113 and 2115 cm^{-1} on the H_2–Au/α-Mn_2O_3 and He–Au/α-Mn_2O_3 catalysts, respectively. In all cases, over the investigated time scale, the location of the Au^0–CO peak remains constant. Moreover, the general shapes of CO/CO_2 related peaks did not change with time, indicating that the nature of adsorbed CO species and thus of the adsorption sites were not modified by the reaction [30].

The integrated intensity of CO, CO_2 and carbonate-related peaks for various Au/α-Mn_2O_3 samples are plotted as a function of time as shown in Fig. 9. The CO and carbonate-related peaks for each sample increased significantly during the first few minutes and then slowly approached a steady state. The intensity of the carbonate related peaks for H_2–Au/α-Mn_2O_3 was much weaker than that of He–Au/α-Mn_2O_3. The strongest carbonate peaks were found on O_2–Au/α-Mn_2O_3, the intensity of which, however, was exceeded by that of He–Au/α-Mn_2O_3 after 60 min. The CO adsorption peak on O_2–Au/α-Mn_2O_3 was much stronger than those on the H_2–Au/α-Mn_2O_3 and He–Au/α-Mn_2O_3 catalysts. As for CO_2 peak evolution, the intensity decreases in the order of O_2–Au/α-Mn_2O_3 > He–Au/α-Mn_2O_3 > H_2–Au/α-Mn_2O_3. In general, the evolution trend of the intensity closely resembled that of the deactivation curve as reported above.

3.5. Discussion

3.5.1. Influence of pretreatment atmosphere on the initial activity

Results obtained in this study clearly demonstrate that the pretreatment atmosphere has a significant influence on both structural and catalytic properties of the Au/α-Mn_2O_3 system in CO oxidation. Pretreatment in inert atmosphere, i.e., He, leads to a gold catalyst with the highest initial activity, which, however, suffers the most severe deactivation with time on stream. In contrast, oxidative pretreatment affords the most stable catalyst while maintaining high activity. The trend of the initial activity for differently pretreated catalysts follows the order of He–Au/α-Mn_2O_3 > O_2–Au/α-Mn_2O_3 > H_2–Au/α-Mn_2O_3, which obviously cannot be simply correlated to the variation of either the oxidation state or the particle size of gold. In fact, XPS results suggested the presence of higher fraction of cationic gold species in the O_2–Au/α-Mn_2O_3 catalyst and TEM images revealed very similar sizes of the gold particles irrespective of the pretreatment conditions.

One possible reason for the different activities of Au catalysts with a similar particle size is the varied Au crystal shapes that resulted from pretreatment under different atmospheres. It is generally accepted that the amount of low-coordinated Au atoms, the key sites for the adsorption and activation of O_2 or CO, depends on both size and shape of the particle [38]. The importance of morphology for Au nanoparticles to obtain a high activity in CO oxidation has been underlined by both theoretical and experimental studies [38–41]. In the present work, although we have no direct evidence on the difference in Au morphology, the variation in the nanoscale Au structures induced by different pretreatments could be inferred from the IR spectra of CO adsorption on the Au/α-Mn_2O_3 catalysts. As shown in Fig. 7, the CO adsorption peak is much weaker on inertly or reductively pretreated Au/α-Mn_2O_3 samples, indicating less exposure of defective gold sites with respective to the O_2–Au/α-Mn_2O_3 sample. This fact may account for the lowest activity of H_2–Au/α-Mn_2O_3 (although in this case the partial encapsulation of Au clusters by partially reduced support may also play a role in blocking the active gold sites as stated in Section 3.2), but cannot explain the highest initial activity of He–Au/α-Mn_2O_3.

Another likely interpretation is related to the surface properties of the support oxide concerning the concentration of oxygen vacancies modified by surface pretreatments. The participation of oxygen vacancies on reducible supports in CO oxidation with Au catalysts was proposed by various groups [42–46]. Applying the technique of quantitative temporal analysis of products (TAPs), Widmann et al. [45] demonstrated that a freshly calcined Au/CeO_2 is only slightly active for CO oxidation and the activity is significantly increased on the removal of about 7% of the surface oxygen, whereas overreduction leads to a lower initial activity. They proposed that the surface oxygen vacancies play an important role in activating the CO oxidation reaction on ceria-supported Au catalysts. As for the Au/α-Mn_2O_3 system in the present study, the highest activity achieved by He-pretreatment may be explained in the same manner. It is reasonable that an optimal amount of surface oxygen vacancies was produced by mild He-pretreatment. In contrast, for the sample pretreated in H_2, the Mn_2O_3 support was overreduced into manganese oxides with lower valence states, leading to deteriorated activity. This assumption is corroborated by the XPS results with respect to the O_L/Mn ratio (see Table 2)

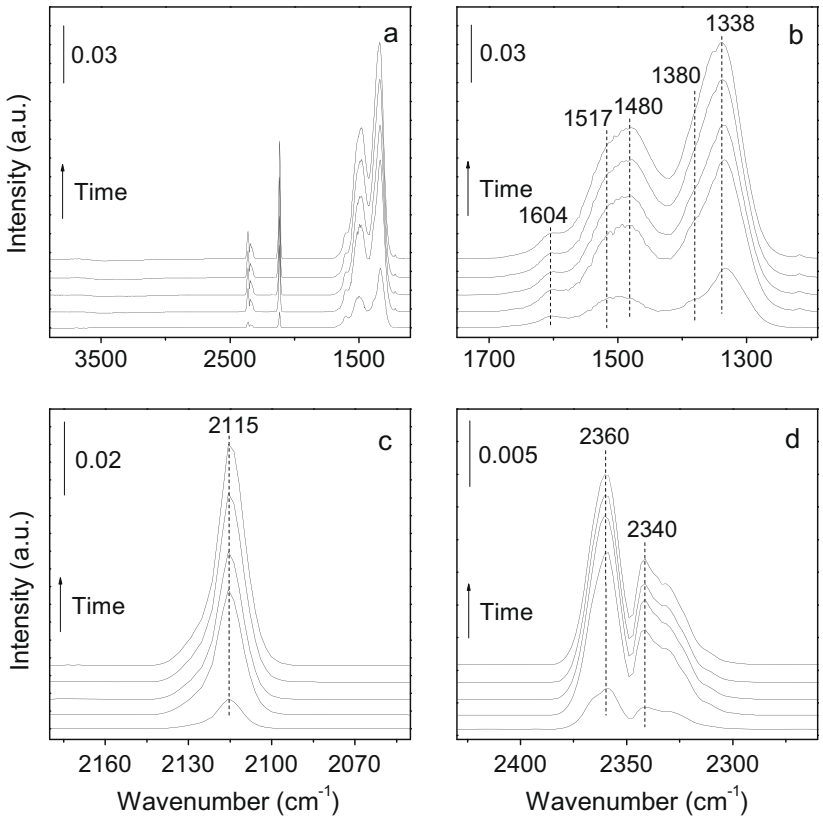

Fig. 8. Sequence of in situ DRIFT spectra recorded during CO oxidation on H_2–Au/α-Mn_2O_3 (reaction times: 2, 10, 20, 60 and 120 min). (a) full spectra, (b) enlarged details of the carbonate region, (c) enlarged details of the C–O stretch region characteristic for CO adsorption and (d) enlarged details of the C–O stretch region characteristic for CO_2.

as well as the XRD pattern (see Fig. 1) of H_2–Au/α-Mn_2O_3, which clearly indicated the presence of Mn_3O_4 phase.

3.5.2. Influence of pretreatment atmosphere on the stability

It has been proposed that two main factors may contribute to the deactivation of Au catalysts in CO oxidation, i.e., the growth of gold particle size induced by the exothermic nature of the reaction and the accumulation of carbonates blocking the active sites [30,31,47–49]. Recently, on investigating the effect of reaction atmospheres on the catalytic performance of a set of unconditioned Au/TiO_2 catalysts, Denkwitz et al. [30] suggested that the dominant reason for the deactivation of Au/TiO_2 is not due to the reaction-induced growth of the very small Au particles (ca. 1.3–1.8 nm), but rather the buildup of surface carbonates on the support during reaction. More recently, by monitoring three activation-deactivation cycles of a Au/MgO catalyst by in situ IR, Hao et al. [48] have shown that the buildup of carbonate-like species on gold particles rather than on the oxide support is responsible for the deactivation. As for the differently pretreated Au/α-Mn_2O_3 catalysts in the present study, investigation by means of in situ DRIFTS clearly shows that substantial amount of surface carbonate species is produced during the reaction, especially for the He–Au/α-Mn_2O_3 and O_2–Au/α-Mn_2O_3 catalysts (Fig. 9). While the rapid deactivation of the He–Au/α-Mn_2O_3 catalyst can be well understood by the continuous accumulation of carbonate-like species, we emphasize that the present DRIFTS data do not provide an explanation for the marginal activity loss of the O_2–Au/α-Mn_2O_3 sample. Moreover, it is noteworthy that the deactivated He–Au/α-Mn_2O_3 catalyst could be regenerated to a large extent along with an even improved stability. All these results strongly suggest that apart from the carbonate accumulation, other factors may also play a crucial role in controlling the deactivation behaviour of the Au/α-Mn_2O_3 catalyst.

It has been reported that the pretreatment of Au/TiO_2 catalyst in oxidative atmosphere can lead to the formation of positive gold species affording a stronger metal–support interaction and better stability against sintering [18]. In addition, a recent model study on the nucleation of Au clusters on TiO_2(1 1 0) surfaces showed a much stronger Au oxide–support adhesion on O-rich Au–support interfaces [50]. Accordingly, based on the results of XPS analysis (Table 2), it is reasonable to speculate that the pretreatment of Au/α-Mn_2O_3 sample in the oxidative atmosphere could also lead to the formation of an oxygen-rich Au–support interface bearing strong bonding strength, which is a likely reason for the superior stability of O_2–Au/α-Mn_2O_3. Indeed, our XPS results clearly indicate that the O_2-pretreated O_2–Au/α-Mn_2O_3 sample is featured with the largest fraction of positively charged gold species. Moreover, the improved stability of the regenerated He–Au/α-Mn_2O_3 can also be well understood based on the fact that oxygen is present in an excess amount in the reactant gas. This is further confirmed by the enhanced signals of the cationic gold species after regeneration, as revealed by the CO adsorption data in Fig. 7.

At this juncture, it is also interesting to point out that there are greater activity differences between catalysts as a function of time on stream (up to about 2 h) than the differences seen between the catalysts as a result of different pretreatments. Notably, the former involve factors of up to 5–6, whereas the latter involve factors of up to only three at the most (see Fig. 5a). The fact that an even larger difference could be identified in the final steady activity allows concluding that the surface pretreatment can have profound influence on the intrinsic activity of the Au/α-Mn_2O_3 system. Such catalytic characteristic could be of great importance for a potential practical application. While further work is needed to fully understand such a remarkable pretreatment-dependent catalytic behaviour, it is important to remark that the steady activity can be well correlated to the significant differences in the corresponding CO_{ad}

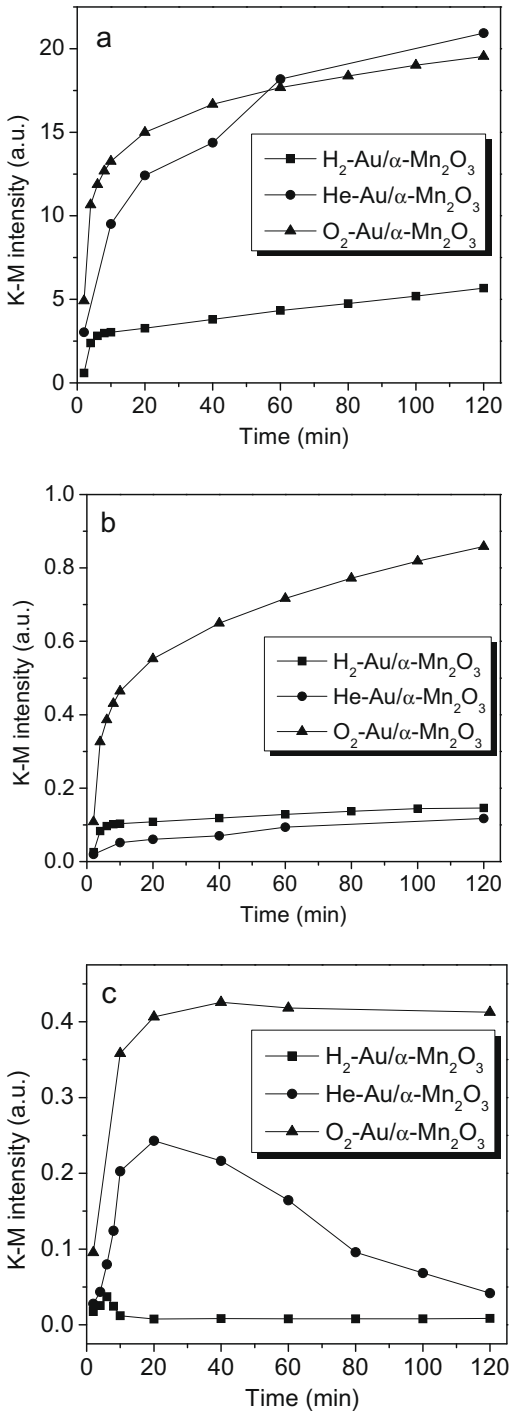

Fig. 9. Evolution of the DRIFT signals characteristic for (a) carbonate, (b) CO adsorption and (c) CO_2 as function of time during CO oxidation.

coverages on various working catalysts, as indicated by the peak intensity of adsorbed CO (see Fig. 9b). Similar correlations have also been adopted by Denkwitz et al. to explain the evolution trend of the activity of Au/TiO_2 catalyst in CO oxidation [30]. In other words, the steady state activity is mainly determined by the amount of the active gold sites available for CO adsorption.

Although the main purpose of this paper was to present a detailed investigation of the structural variation of both Au and α-Mn_2O_3 phases in the specific Au/α-Mn_2O_3 catalyst system upon pretreatment under different atmospheres, we would like to comment here on the practical implications of the present results. It is well known that many supported metal nanoparticles, such as Cu [51], Pt [52], Pd [53] and Rh [54], can undergo substantial geometric/electronic changes when treated in oxidative or reductive atmosphere at moderate temperatures. In the specific case of supported gold nanoparticles, such geometric/electronic variations may also occur upon various pretreatments, thus leading to greatly modified catalytic properties. While it is not yet possible to achieve a complete understanding of the catalytic origin and the very nature of the Au species for CO oxidation [55,56], results obtained in this study indicate that the pretreatment–dependent catalytic behaviour of the Au/α-Mn_2O_3 system arises largely from the structure-sensitivity of the metal–support interface. We believe that this rationalization may be readily extended to gold supported on other reducible oxides [3–5], over which significantly discrepant catalytic activities have been frequently identified with even the same composition or similar Au particle size. This highlights new opportunities in the development of highly active and stable Au-based catalysts for a range of catalytic applications.

4. Conclusions

In this study, the effect of the pretreatment atmosphere on the structural and catalytic properties of the Au/α-Mn_2O_3 system in the low temperature CO oxidation reaction was investigated. TEM results showed that the pretreatment atmosphere had a negligible effect on the gold particle size distribution, while XPS revealed a higher fraction of positively charged gold species in the catalyst pretreated with O_2. It is proposed that the highest initial activity obtained on $He–Au/\alpha$-Mn_2O_3 is due to the moderate formation of surface oxygen vacancies prior to the reaction, while the overreduction of the oxide support evidenced by XRD may account for the lowest activity of $H_2–Au/\alpha$-Mn_2O_3. As compared with the He-pretreated sample, the superior stability of $O_2–Au/\alpha$-Mn_2O_3 has been attributed to its enhanced metal–support synergy rather than suppressed accumulation of carbonate-like surface species as revealed by in situ DRIFTS studies.

Acknowledgments

This work was supported by the National Natural Science Foundation of China (20633030, 20721063 and 20873026), the National Basic Research Program of China (2003CB615807), the National High Technology Research and Development Program of China (2006AA03Z336), Science and Technology Commission of Shanghai Municipality (08DZ2270500, 07QH14003) and the Committee of the Shanghai Education (06SG03).

References

[1] G.C. Bond, D.T. Thompson, Catal. Rev. Sci. Eng. 41 (1999) 319.
[2] A.S.K. Hashmi, G.J. Hutchings, Angew. Chem. Int. Ed. 45 (2007) 7896.
[3] M.M. Schubert, S. Hackenberg, A.C. van Veen, M. Muhler, V. Plzak, R.J. Behm, J. Catal. 197 (2001) 113.
[4] M. Haruta, S. Tsubota, T. Kobayashi, H. Kageyama, M.J. Genet, B. Delmon, J. Catal. 144 (1993) 175.
[5] S. Carrettin, P. Concepción, A. Corma, J.M. Lopez Nieto, V.F. Puntes, Angew. Chem. Int. Ed. 43 (2004) 2538.
[6] L.C. Wang, X.S. Huang, Q. Liu, Y.M. Liu, Y. Cao, H.Y. He, K.N. Fan, J.H. Zhuang, J. Catal. 259 (2008) 66.
[7] L.C. Wang, Q. Liu, X.S. Huang, Y.M. Liu, Y. Cao, K.N. Fan, Appl. Catal. B: Environ. 88 (2009) 204.
[8] B.K. Min, C.M. Friend, Chem. Rev. 107 (2007) 2709.
[9] F. Moreau, G.C. Bond, A.O. Taylor, J. Catal. 231 (2005) 105.
[10] R. Zanella, C. Louis, Catal. Today 107–108 (2005) 768.
[11] F. Boccuzzi, A. Chiorino, M. Manzoli, P. Lu, T. Akita, S. Ichikawa, M. Haruta, J. Catal. 202 (2001) 256.
[12] M. Haruta, M. Daté, Appl. Catal. A: Gen. 222 (2001) 427.
[13] T.V.W. Janssens, A. Carlsson, A. Puig-Molina, B.S. Clausen, J. Catal. 240 (2006) 108.
[14] S.D. Gardner, G.B. Hoflund, M.R. Davidson, H.A. Laitinen, D.R. Schryer, B.T. Upchurch, Langmuir 7 (1991) 2140.

[15] S.D. Gardner, G.B. Hofland, B.T. Upchurch, D.R. Shriver, E.J. Kielen, J. Schyer, J. Catal. 129 (1991) 114.
[16] S. Tsubota, D.A.H. Cunningham, Y. Bando, M. Haruta, Stud. Surf. Sci. Catal. 91 (1995) 227.
[17] E.D. Park, J.S. Lee, J. Catal. 186 (1999) 1.
[18] K.Y. Ho, K.L. Yeung, J. Catal. 242 (2006) 131.
[19] K. Ramesh, L. Chen, F. Chen, Z. Zhong, J. Chin, H. Mook, Y.F. Han, Catal. Commun. 8 (2007) 1421.
[20] R. Zanella, S. Giorgio, C.R. Henry, C. Louis, J. Phys. Chem. B 106 (2002) 7634.
[21] S.T. Daniells, A.R. Overweg, M. Makkee, J.A. Moulijn, J. Catal. 230 (2005) 52.
[22] A. Corma, H. Garcia, Chem. Soc. Rev. 37 (2008) 2096.
[23] K. Ramesh, L. Chen, F. Chen, Y. Liu, Z. Wang, Y.-F. Han, Catal. Today 131 (2008) 477.
[24] L. Guczi, D. Horváth, Z. Pászti, L. Tóth, Z.E. Horváth, A. Karacs, G. Petõ, J. Phys. Chem. B 104 (2000) 3183.
[25] S.J. Lee, A. Gavriilidis, Q.A. Pankhurst, A. Kyek, F.E. Wagner, P.C.L. Wong, K.L. Yeung, J. Catal. 200 (2001) 298.
[26] F. Boccuzzi, A. Chiorino, M. Manzoli, D. Andreeva, T. Tabakova, J. Catal. 188 (1999) 176.
[27] R. Leppelt, B. Schumacher, V. Plzak, M. Kinne, R.J. Behm, J. Catal. 244 (2006) 137.
[28] F.C. Meunier, D. Reida, A. Goguet, S. Shekhtman, C. Hardacre, R. Burch, W. Deng, M. Flytzani-Stephanopoulos, J. Catal. 247 (2007) 277.
[29] F.C. Meunier, A. Goguet, C. Hardacre, R. Burch, D. Thompsett, J. Catal. 252 (2007) 18.
[30] Y. Denkwitz, Z. Zhao, U. Hörmann, U. Kaiser, V. Plzak, R.J. Behm, J. Catal. 251 (2007) 363.
[31] M. Azar, V. Caps, F. Morfin, J.-L. Rousset, A. Piednoir, J.-C. Bertolini, L. Piccolo, J. Catal. 239 (2006) 307.
[32] M.M. Schubert, A. Venugopal, M.J. Kahlich, V. Plzak, R.J. Behm, J. Catal. 222 (2004) 32.
[33] M. Haruta, Catal. Today 36 (1997) 153.
[34] M.A. Bollinger, M.A. Vannice, Appl. Catal. B: Environ. 8 (1996) 417.
[35] F. Boccuzzi, A. Chiorino, S. Tsubota, M. Haruta, J. Phys. Chem. 100 (1996) 3625.
[36] J.-D. Grunwaldt, M. Maciejewski, O.S. Becker, P. Fabrizioli, A. Baiker, J. Catal. 186 (1999) 458.
[37] B. Schumacher, Y. Denkwitz, V. Plzak, M. Kinne, R.J. Behm, J. Catal. 224 (2004) 449.
[38] N. Lopez, J.K. Nørskov, T.V.W. Janssens, A. Carlsson, A. Puig-Molina, B.S. Clausen, J.-D. Grunwaldt, J. Catal. 225 (2004) 86.
[39] N. Lopez, T.V.W. Janssens, B.S. Clausen, Y. Xu, M. Mavrikakis, T. Bligaard, J.K. Nørskov, J. Catal. 223 (2004) 232.
[40] R. Zanella, C. Louis, C. Shin, S. Giorgio, C.R. Henry, J. Catal. 222 (2004) 357.
[41] S. Giorgio, M. Cabié, C.R. Henry, Gold Bull. 41 (2008) 167.
[42] H. Liu, A.I. Kozlov, A.P. Kozlova, T. Shido, Y. Iwasawa, Phys. Chem. Chem. Phys. 1 (1999) 2851.
[43] L. Guczi, D. Horvath, Z. Paszti, G. Peto, Catal. Today 72 (2002) 101.
[44] B. Grzybowska, Catal. Today 112 (2006) 3.
[45] D. Widmann, R. Leppelt, R.J. Behm, J. Catal. 251 (2007) 437.
[46] B. Yoon, H. Häkkinen, U. Landman, A.S. Wörz, M. Antonietti, S. Abbet, K. Judai, U. Heiz, Science 307 (2005) 403.
[47] C.H. Kim, L.T. Thompson, J. Catal. 230 (2005) 66.
[48] Hao, M. Mihaylov, E. Ivanova, K. Hadjiivanov, H. Knözinger, B.C. Gates, J. Catal. 261 (2009) 137.
[49] T.A. Ntho, J.A. Anderson, M.S. Scurrell, J. Catal. 261 (2009) 94.
[50] D. Matthey, J.G. Wang, S. Wendt, J. Matthiesen, R. Schaub, E. Lægsgaard, B. Hammer, F. Besenbacher, Science 315 (2007) 1692.
[51] P.L. Hansen, J.B. Wagner, S. Helveg, J.R. Rostrup-Nielsen, B.S. Clausen, H. Topsoe, Science 295 (2002) 2053.
[52] Y. Nagai, K. Dohmae, Y. Ikeda, N. Takagi, T. Tanabe, N. Hara, G. Guilera, S. Pascarelli, M.A. Newton, O. Kuno, H. Jiang, H. Shinjoh, S. Matsumoto, Angew. Chem. Int. Ed. 47 (2008) 9303.
[53] A. Suzuki, Y. Inada, A. Yamaguchi, T. Chihara, M. Yuasa, M. Nomura, Y. Iwasawa, Angew. Chem. Int. Ed. 42 (2003) 4795.
[54] M.A. Newton, C. Belver-Coldeira, A. Martínez-Arias, A.M. Fernandez-García, Nat. Mater. 6 (2007) 528.
[55] G.C. Bond, C. Louis, D.T. Thompson, Catalysis by Gold, Imperial College Press, London, 2006. p. 193.
[56] G.C. Bond, D.T. Thompson, Gold Bull. 33 (2000) 41.